Developing Solution Processable Distributed Bragg Reflectors for Polaritonic Applications

Master's thesis
University of Turku
Materials Engineering
2024
B.Sc. Michael A. Papachatzakis
Examiners:
Prof. Konstantinos S. Daskalakis
Mr. Ahmed Abdelmagid

The originality of this thesis has been checked in accordance with the University of Turku quality assurance system using Turnitin Originality Check service.

UNIVERSITY OF TURKU
Department of Mechanical and Materials Engineering

Student, Michail A. Papachatzakis

Developing Solution Processable Distributed Bragg Reflectors for Polaritonic Applications

Master's thesis, 49 pp.
Materials Engineering
May 2024

In the pursuit of advancing electromagnetic confinement and manipulating physical phenomena, Quantum Electrodynamics and polaritons have emerged as pivotal concepts. Polaritons, which result from strong coupling between light and dipole-carrying excitations like excitons, play crucial roles across various scientific disciplines, including chemistry, quantum computing, and optoelectronics. Optical microcavities, defined by their resonance and quality factor (Q-factor), are key to enhancing polariton formation. While metal-clad microcavities and dielectric structures like Distributed Bragg Reflectors (DBRs) are prevalent, their fabrication through Physical Vapor Deposition (PVD) poses challenges in cost and complexity. Consequently, there is a growing interest in solution-processable methods for DBRs and microcavities, which promise simplicity, cost-effectiveness, and scalability. This thesis explores the development of solution-processable DBRs and microcavities using an in-house automated dip-coater. By alternating PVA/TiOH as high refractive index material and Nafion as low refractive index material, we manage to fabricate photonic structures such as a simple DBR structure, a fully dielectric microcavity, and a hybrid microcavity integrating solution-processed DBRs with PVD-deposited metal mirrors and TDAF excitonic materials. Overall, this research demonstrates the feasibility and effectiveness of solution-processable photonic structures in enabling practical applications of polaritons, thereby expanding the possibilities for future optoelectronic devices.

Keywords: Polaritons, Distributed Bragg Reflectors, Microcavities, OLEDs.

Acknowledgements

I am sincerely grateful to several individuals whose contributions made this research possible. Emilia Palo deserves special thanks for her thin-film optimization expertise and Hassan Quereshi's work in k-space spectroscopy. Ahmed Abdelmagid and Manish Kumar played crucial roles in the preparation of hybrid microcavities, contributing to the experimental success of this project. Finally, I sincerely thank my supervisor, Konstantinos Daskalakis, for his support, guidance, and access to the Luminous Material Devices laboratories at the University of Turku. Their collective efforts and expertise have made this work possible, and I am truly thankful for their contributions.

Contents

1 Preface

In the quest to understand the physics under electromagnetic confinement and to manipulate physical phenomena for improved parameters, the concept of Quantum electrodynamics and polaritons emerged. There are many different types of polaritons, and the distinction between them is the dipole-carrying excitation that is strongly coupled with light. Polaritons find use in many fields of science such chemistry, [1–3] quantum computing, [4, 5] optoelectronics [6] etc. In the case of optoelectronics, polaritons show particular interest in photovoltaics [7–13], sensors [14–19] , optical gates [20, 21] , lasers [22–27] and OLEDs [28, 29]. In light emitting devices such as lasers and OLEDs, polaritons are promised for improved and more efficient devices such as -among others- low lasing threshold voltages in lasers [30], improved outcoupling and light emission in OLEDs [31, 32] with the most noteworthy effect the well-known Purcell enhancement [33, 34]. Polaritons are formed in the strong light-matter coupling regime between light and an exciton. In crystalline semiconductors, excitons exist for a short period of time, and usually, they are thermally dissociated, rendering polariton formation at room temperature difficult. Thus, in order to prevent the exciton of dissociating, cryogenic temperatures are required, limiting their potential in real-world applications. Following the invention of organic semiconductors, and due to the strong binding energies, room temperature polaritons were quickly realized. Polaritons can exist in many photonic structures such as waveguides [35–39], plasmonic structures [40–44] and optical microcavities with the latter being the most used photonic structure. An optical microcavity is an electromagnetic resonator of light that consists of two highly reflective planes separated at a comparable distance of the wavelength of the standing electromagnetic wave [45]. The quality factor (Q-factor) of microcavity is a metric that defines how efficient the microcavity is storing electromagnetic radiation. The Q-factor plays a crucial role in forming polaritons, and a lossy microcavity is generally undesirable.

Thus, the highly reflective faces are usually made of metals (metal-clad microcavity) or dielectric photonic structures such as distributed Bragg reflector (DBR) microcavities. DBRs are photonic structures composed of dielectric materials of high and low refractive index materials sandwiched together. A naive explanation of the reflection mechanism of a DBR is the constructive and destructive interference created at the interfaces of the layers. The deposition of such mirrors usually involves a physical deposition system (PVD), a highly sophisticated and expensive process, limiting the polariton research in terms of speed and feasibility.

Solution processable methods are generally desirable due to the simplicity of deposition, low cost, and speed, enabling accelerated research. Research groups can utilize PVD in conjunction with solution-processed methods when cross-referencing is required. Furthermore, new and emerging scientific groups can adopt solution-processed methods. Thus, in this thesis, the process of solution-processable DBRs and microcavities is described. The solution-processed DBRs were made using a modified dip-coater that automatically alternated the dielectric solutions and annealed the sample. The high refractive index material used is a Titanium hydroxide (TiOH) in a poly(vinyl alcohol) (PVA) matrix, whereas the low refractive index material used is Nafion®. In this thesis, three photonic structures were implemented and tested. The first one is a simple DBR consisting of 6-pairs. The second structure was a fully dielectric microcavity, which implemented a 6+6 pair of DBRs with a dual deposition of the PVA/TiOH solution in order to create the desired spacer of λ /2 thickness. The DBRs achieved a reflectance of more than 90%, whereas the fully dielectric microcavity achieved a Q-factor of >91, which is higher than a metal-clad microcavity [46, 47]. Finally, a hybrid microcavity was fabricated consisting of a solution-processed DBR, TDAF as the excitonic material in the cavity, and finally, a metal mirror deposited using PVD. The TDAF hybrid microcavity successfully proved the polaritonic behavior with the solution-processable approach,

and the lower polariton was shown.

2 Theory

In this section, the basic knowledge will be provided to clarify the scope of this thesis. First, an introduction to the organic emitters will be presented. Subsequently, we will introduce photonic structures, explaining how they create polaritons and the reasons behind their formation.

2.1 Organic light emitters

Organic light emitters are organic molecules or organic polymers that are usually used in Organic Light Emitting Diodes (OLEDs) and are able to emit light in the visible region. Due to generally being direct band-gap semiconductors, when an electron and a hole are recombined in the organic semiconductor, energy can be emitted in the form of light. Organic emitters have drawn a lot of attention due to the huge market of OLED displays, which are mostly used in premium products, namely mobile phones, televisions, and, to a lesser extent, general illumination. One main advantage that organic emitters can pose is that they are environmentally friendly compared to other lighting technologies that we currently have. Organic emitters pose a lot of benefits, such as ease of deposition, color tunability, etc, but they pose some disadvantages as well, mainly low efficiency and limited lifetime. Another problem that organic emitters pose is due to their thin layers, is difficult to out-couple the produced light. Photonic structures such as microcavities and polariton research can improve those aspects, bridging the gap between research and commercialization. Thus, further research needs to be done in order to improve their efficiencies and lifetime. Currently, there are three generations of organic light emitters. In this thesis, we are not fabricating an OLED, but a photonic structure in order to accelerate the research in improving the aspects of an OLED with photonics.

2.1.1 First generation: Fluorescent emitters

The first generation of organic emitters are the fluorescent emitters. The fluorescent materials can emit only through the singlet state. Under electrical excitation, the singlet emission accounts for 25% of maximum efficiency. The rest is occupied by the triplet, which exhibits a non-radiative emission. Thus, 75% of the total energy is lost as heat. In this thesis, the emitter used was the TDAF, which is a first-generation material.

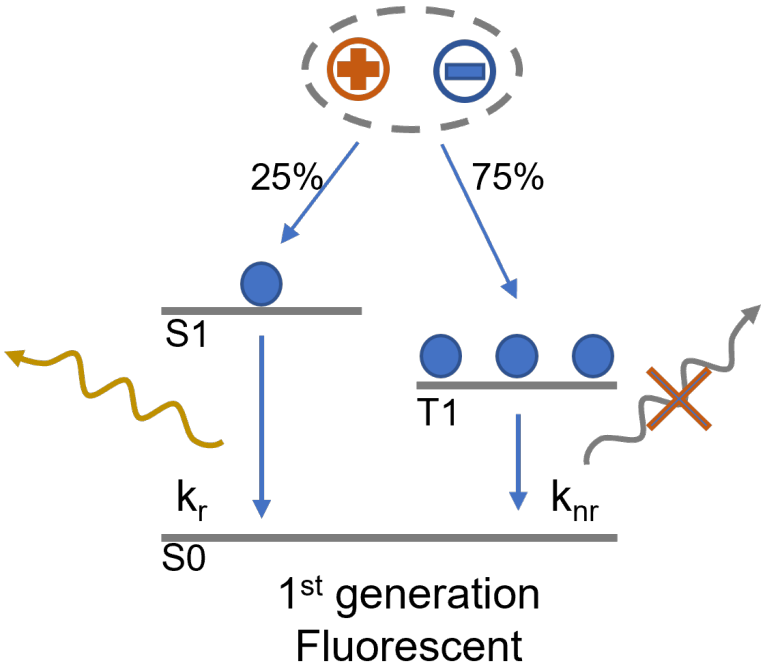

Figure 1. The first generation materials showing the paths of the charges. The radiative singlet emission accounts for 25%. The non-radiating triplet emission accounts for 75%.

2.1.2 Second generation: Phosphorescent emitters

The second generation of organic emitters is the phosphorescent emitters. These can utilize the triplets in order to produce light by triplet harvesting through a mechanism called intersystem crossing. These emitters can theoretically achieve 100% internal quantum efficiency. Even though these emitters can have significantly

higher efficiencies on paper, they are challenging in practice. Furthermore, the emitters are using heavy metal atoms in heavy metal complexes in order to achieve the triplet harvesting, defeating the purpose of environmentally friendly materials

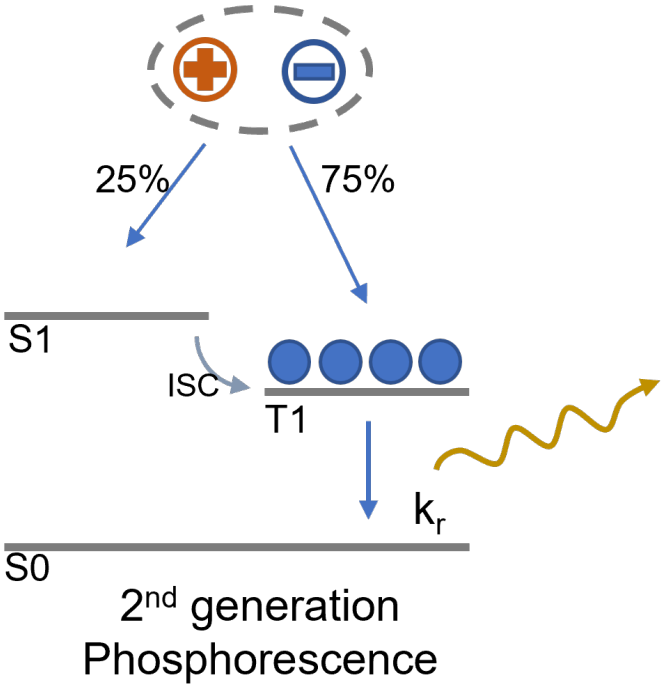

Figure 2. The second generation materials showing the paths of the charges. The radiative singlet and triplet emission accounts for 100%. This is achieved by triplet harvesting.

2.1.3 Third generation: Thermally activated delayed fluorescent emitters

The third generation of organic emitters is the thermally activated delayed fluorescent emitters (TADF). These emitters don't incorporate the heavy metal atom; thus, they are generally considered more ecological. These emitters harvest the triplets using a mechanism called reverse intersystem crossing. Essentially, these emitters have singlet and triplet energy levels that are sufficiently close, allowing excitons to transition into the singlets through thermal up-conversion, as illustrated in Figure 3

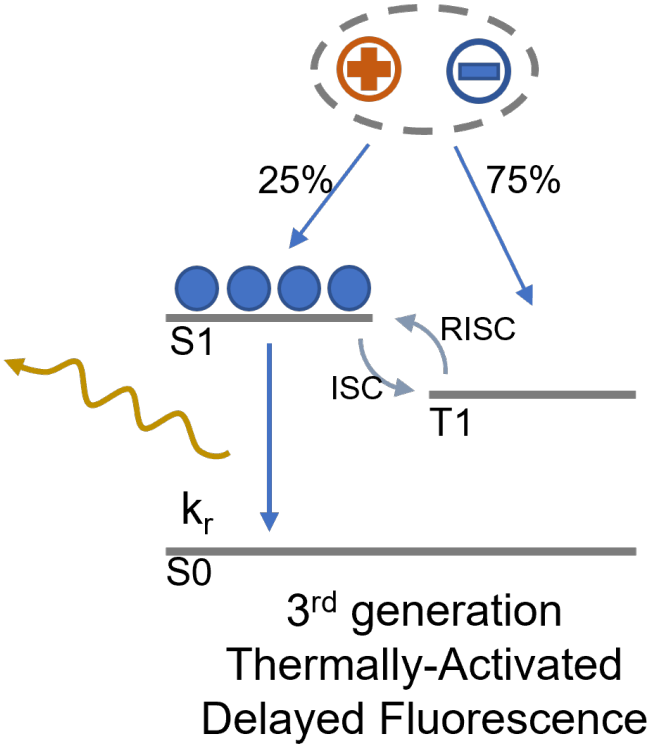

Figure 3. The third generation materials showing the paths of the charges. The radiative singlet emission accounts for 100%. This is achieved by triplet harvesting through the reverse intersystem crossing by thermal up-conversion.

2.2 Distributed Bragg reflectors

Distributed Bragg reflectors (DBRs) are multilayer photonic structures that exploit the constructive and destructive interference of light in order to produce highly reflective and well-defined windows in the spectrum. This window of wavelengths is called a stopband. Outside of the stopband, there are periodic transmissive windows, which are called Bragg-modes (figure 5). The photonic structure is composed of alternate layers of high and low refractive index transparent materials. Equations 1 and 2 describe the maximum reflectivity and the stopband width in the normal incidence, respectively [48]. The n_a and n_s are the refractive index of the surrounding medium (air) and the refractive index of the substrate, respectively, whereas the n_H and n_L are the high and low refractive index of the Bragg stack. Finally, the N is

the number of pairs and λ_0 the central wavelength of the stopband [49, 50].

$$R_{HR,max} = \left(\frac{1 - (\frac{n_s}{n_a}\frac{n_H}{n_L})^{2N}}{1 + (\frac{n_s}{n_a}\frac{n_H}{n_L})^{2N}} \right)^2 \tag{1}$$

$$\frac{\Delta\lambda_0}{\lambda_0} = \frac{4}{\pi} \arcsin\left(\frac{n_H - n_L}{n_H + n_L} \right) \tag{2}$$

In the figure 4, a high-level illustration of a light ray at an angle θ is shown. In reality, a DBR stack does not reflect in this way. The way a DBR reflects and transmits can be described with complex physics, which involves wave propagation in a medium, and it is very hard to depict in a simple figure. For example, a DBR exhibits angle-dependence, which is not described in equations 1 and 2. Angle-dependence is the shifting of the stopband with the angle. This can be seen in the experimental section in the figure 21. Nevertheless, the simple equations above can describe the system and they are adequate for this thesis. For a more involved explanation, refer to the *Electromagnetic Waves and Antennas* book [49].

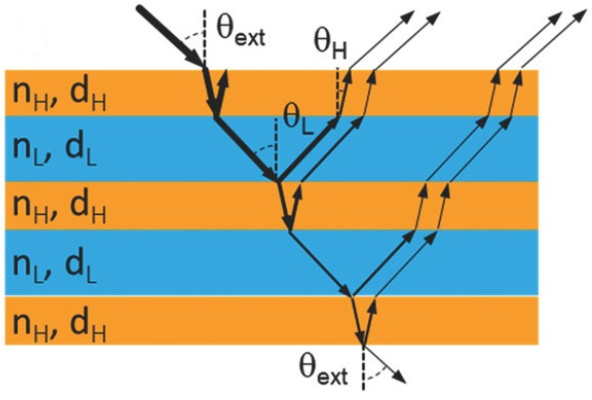

Figure 4. A visual illustration of the path and the reflections take are taking place inside the DBR structure. *Reprinted with permission. [51]*

The optical thickness of a DBR is defined as $\lambda/4n$. Thus, the thickness of each layer for a specific stopband λ_0 depends in its refractive index. Due to almost lossless reflection, DBRs are mostly used as high-quality mirrors while the Bragg modes are usually not utilized, although there are cases in which they have been utilized as transmitting windows in photonic devices [52].

In the figure 5 the relation between the amount of pairs N to the stopband shape and reflectivity can be seen. The higher the numbers the more reflective the stopband is. In addition to that, the larger the refractive index difference the sooner high reflectivity can be achieved. In a real-world scenario, materials absorb; thus, a low number of pairs and high refractive index difference would be desirable in order to minimize the losses.

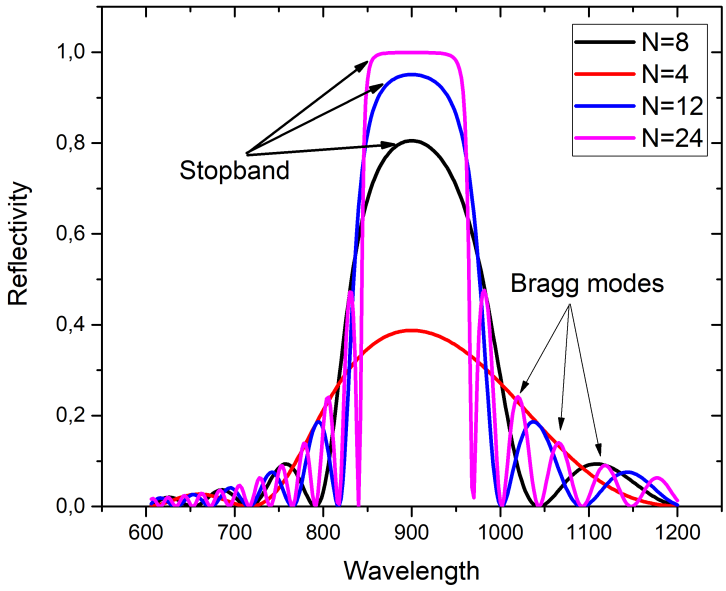

Figure 5. A simulation of the stopband shape and definition versus the number of pairs. The Bragg modes can be easily seen in this figure, the valleys of the Bragg modes are areas which are highly transmissive. The high refractive index is $n_H = 3.6$ and the low refractive index is $n_L = 3$ with no losses.

2.3 Microcavities

An optical microcavity is an electromagnetic resonator of light that confines an electromagnetic wave in a small volume. Microcavities can be constructed in many different geometries [53, 54], but in this section, the planar microcavity will be described. A planar microcavity is usually composed of two highly reflective planes separated at a comparable distance of the wavelength of the standing electromagnetic wave [45] figure 6.

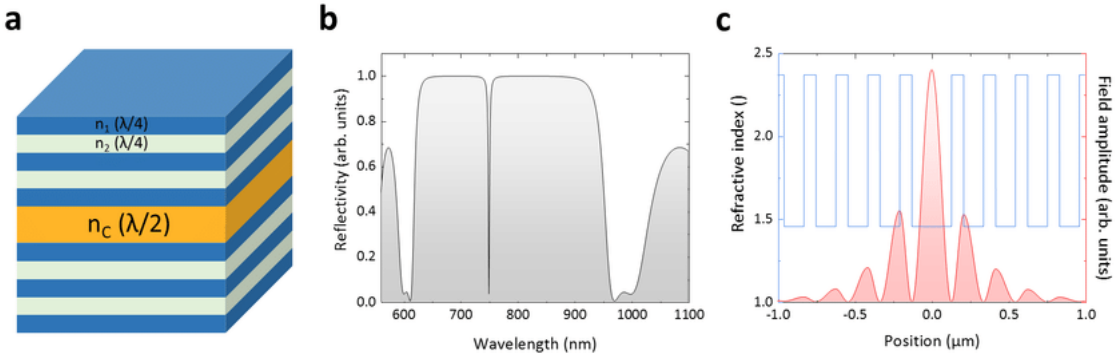

Figure 6. a) A depiction of a microcavity composed from DBRs. The cavity thickness is of $\lambda/2$ and light can enter from the top and it is trapped. Inside the microcavity a static wave node is created, achieving strong electromagnetic confinement. b) Reflection of the microcavity. The narrow spectral absorption line indicates a high-Q microcavity. c) The electromagnetic confinement can be observed with the red indicating an increase in the field intensity. [55]

Microcavities are used in lasers [56], quantum optics [57], sensors [58] etc. A notable example is the vertical-cavity surface-emitting laser which is a highly used semiconductor laser, achieving low-threshold voltages and small footprints. The microcavity quality factor (Q-factor) describes how lossy the cavity is. A microcavity with a high Q-factor is usually desirable because it can achieve strong electromagnetic confinement. A perfect microcavity will exhibit an infinite Q-factor, which will imply that the electromagnetic wave will exist in the cavity forever. Furthermore, a high-Q microcavity will exhibit a very narrow absorption. Microcavities usually accommodate a material that can alter its properties under strong electromagnetic

confinement conditions and, thus, are almost never empty.

2.4 Coupled harmonic oscillators and strong coupling

A coupled harmonic oscillator is a fundamental part of physics [59] and can be found in every discipline in science, from mechanical systems, electrical circuits, and molecular vibrations to the explanation of quantum phenomena. Coupled harmonic oscillators are important in understanding the polaritons and the transfer of energy in quantum systems.

When two harmonic oscillators with the same natural frequency share the same medium and are closely coupled with each other, they can transfer energy bidirectionally through that medium. This principle applies to all the disciplines but with different forms of energy and means of transferring that energy are involved. In the case of a mechanical system, a simple harmonic oscillator can be made from two oscillators composed of two masses and two springs connected with a coupling spring; the coupling spring is the means of transferring the energy between those two. In the case of electrical circuits, a harmonic oscillator can be made with two LC circuits in close proximity to each other, whereas the transferring of energy happens with a mutual magnetic field or electric field. The mechanical system will be explained first for conceptual clarity. Figure 7b illustrates a mechanically coupled harmonic oscillator system, where the motion can be described using Newton's second law. In this system, mass M_A is attached to spring k_A and coupled through a coupling spring k_C to mass M_B, which is attached to spring k_B. This configuration results in interactions between the masses and springs, leading to coupled oscillations. Applying Newton's second law to each mass results in two coupled differential equations that govern the system's dynamics, accounting for the forces exerted by the springs and the coupling mechanism. This setup results in two differential equations [60]:

$$M_A\ddot{x}_A + k_A x_A + k_C(x_A - x_B) = 0 \tag{3}$$

$$M_B\ddot{x}_B + k_B x_B - k_C(x_A - x_B) = 0 \tag{4}$$

Solving the differential equations results in two modes:

$$\omega_\pm = \frac{1}{2}\left(\omega_A + \omega_B \pm \sqrt{(\omega_A - \omega_B)^2 + 4\Omega^2}\right) \tag{5}$$

When resonance occurs there are two modes created as noted in the figure 7a as ω_+ and ω_-. The normal mode splitting is the separation between those two modes (denoted with Ω), and it is dependent on the coupling strength (k_C). In short, the normal modes in this mechanical system are the symmetric mode, in which the motion of the masses is in phase (oscillate in the same exact direction), and anti-symmetric mode, in which the motion of the masses is out-of-phase (oscillate in exactly opposite direction). When the dissipation in a coupled harmonic oscillator system is smaller than the coupling strength, then the said system is in a strong coupling regime. In this regime the characteristic frequency splitting is observed or anticrossing.

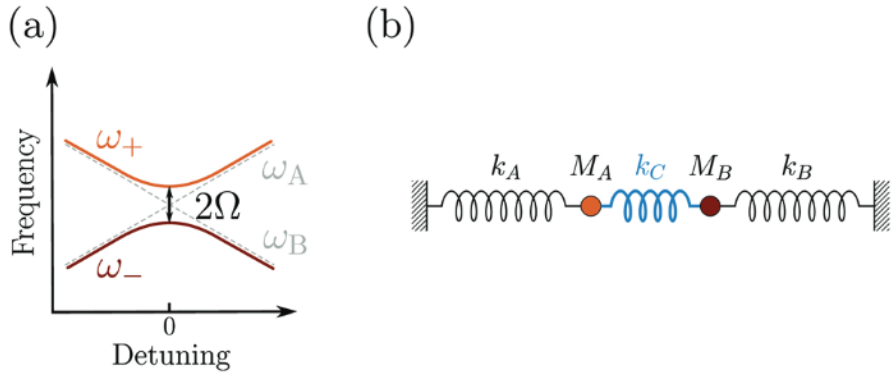

Figure 7. a) The two modes ω_+ and ω_- versus the detuning which is controlled by the k_C. b) An illustration of the mechanical system composed of two harmonic oscillators coupled with a coupling spring k_C [60]

The concept of this simple mechanical system can be easily visualized. Thus, it is important to understand coupled harmonic oscillators. Almost the same fundamental physical concept can be applied to quantum phenomena, albeit with more complex equations. The quantum harmonic oscillator will be explained here superficially. For a quantum harmonic oscillator, instead of a physical connection, the coupling medium is the electric field[61] as expressed by:

$$U_{(x)} = \frac{1}{2}m\omega^2 x^2 \tag{6}$$

In quantum mechanics, the couple harmonic oscillator is quantized and the displacements are expressed by the Hamiltonian. The Hamiltonian of the system describes the sum of the kinetic and potential energy. The equation 7 described such a system, where k is the coupling constant, p is the conjugation momentum, and finally, x is the quantized displacement.

$$H = \frac{p_1^2}{2m} + \frac{p_2^2}{2m} + \frac{1}{2}kx_1^2 + \frac{1}{2}kx_2^2 + \frac{1}{2}k'(x_1 - x_2)^2 \tag{7}$$

Excitonic materials such as organic emitters have an absorption maxima where the exciton most likely exists, coupling near this region with a microcavity results in strong coupling. When light interacts with matter in the strong coupling regime then the energy exchange rate between excitons and photons is faster than the rate of energy dissipation. This creates the new quasi-particles that exhibit characteristics of both light and matter, called polaritons.

2.4.1 Polaritons

Polaritons are quasi-particles that are formed under strong electromagnetic confinements. They are a result of strongly coupling the optical mode and an exciton. The strong coupling can be achieved -as is the case with this thesis- in a microcavity. As previously explained, strong coupling results in the emergence of two modes. In the case of polaritons, these modes are referred to as the upper polariton (UP) and the lower polariton (LP). The Hamiltonian describing the coupled photon-exciton system is given by [62]:

$$H = \hbar\omega_c a' + \hbar\omega_X b'b + \hbar g(a'b + ab') \tag{8}$$

Where the a,b, and a',b' are the annihilation and creation operators for the photons and excitons, respectively. The ω_c and ω_X are the frequencies of the photos and exciton, finally, g is the coupling strength. The difference between ω_c and ω_X is the detuning. The photon frequency is controlled by the cavity whereas the exciton frequency is controlled by the material. For a material to exhibit polaritons it needs to be excitonic. That means that needs to have high binding energy in order for the exciton to exist for a considerable amount of time. If the exciton dissociates, then

no coupling can occur because, by that time, the exciton is simply a free electron and a free hole. This is the reason why the polariton research is mainly focused on organic materials.

3 Experimental

In this thesis certain experimental parameters were already optimized by other members of the LMD group. For instance, the polymer solution concentration and chemical synthesis. Further optimization was needed in order to produce the high-quality films and the repeatability needed to be able to achieve high Q-factors in the microcavities which was necessary in order to achieve strong coupling. Thus, a lot of attention was focused in order to optimize the fabrication procedure in such a way that it would produce DBRs of an acceptable quality both in terms of stopband and reflectivity. In this section, a concise description of the processes involved will be provided, along with the process improvements done in each step. An additional challenge that comes with almost all the polymers is the high absorption in the near-UV and upper region. This rendered this work particularly challenging since the absorption of the organic fluorescent TDAF (2,7-Bis[9,9-di(4-methylphenyl)-fluoren-2-yl]-9,9-di(4-methylphenyl)fluorene) emitter is in the near-UV region [63]. Nevertheless, TDAF was a promising candidate since it has the ability to exhibit polaritons [26] under a strong coupling regime even in relatively low Q-factors.

3.1 High contrast refractive index polymers

The fabrication of high-quality solution-processed DBRs requires a careful selection of transparent polymers in order to achieve surface layer compatibility, low absorption, etc. For our research, we needed two highly transparent materials with high refractive index difference Δn between them in order to be able to produce a sharp stopband with as few layers as possible. The material selection was Nafion and TiOH in a PVA matrix. These polymers showed good surface layer compatibility and uniformity. It is noteworthy that even though the solvents used to dissolve/dilute the polymers were not orthogonal, the polymer layers were robust enough not to be dissolved immediately, thus exhibiting non or insignificant intermixing. The deposition

parameters in the dip-coater were kept constant and in order to fine-tune the thickness, the concentration of the solution was changed. The deposition parameters are as follows; (a) First the substrate was lowered and maintained in the solution for 10s in order to sufficiently wet the surface, (b) afterward the substrate was raised from the solution at a speed of 40mm/min and (c) lastly it was dried onto the heater for one and a half minutes at 80°C and left to cooldown for an additional one and a half minute, the whole procedure is depicted in the figure: 8. Finally, this process continued for 12 layers in total for a single DBR stack and 26 layers for a fully dielectric microcavity. For the complete deposition of a single layer, it takes approximately 3 minutes, significantly faster than the PVD deposition.

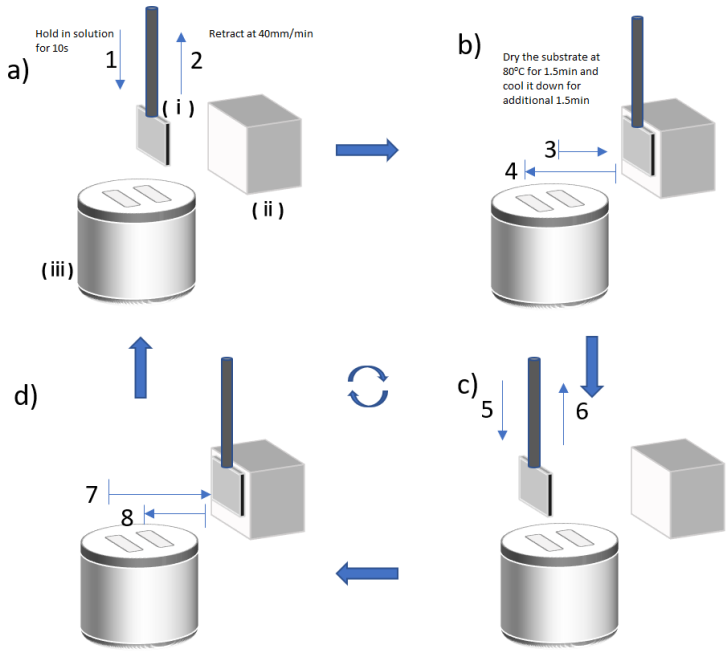

Figure 8. The automated dip-coating process. a.1) The substrate is lowered in the first solution and is left to wet for 10 seconds. a.2) The substrate is retracted at a speed of 40mm/min. b.1) The coated substrate is left to dry at 80°C for one and a half minutes. b.2) The substrate is moved away from the heater and positioned on top of the second solution and left for one and a half minutes in order to let it cool down. c,d) These steps are the same as a,b but are applicable to the second layer.

3.1.1 Nafion preparation

Nafion® is a fluoropolymer-copolymer commonly used as a proton exchange membrane in fuel cells, but in this case, it perfectly serves the purpose of the low refractive index material. Furthermore, Nafion showed excellent compatibility with the whole dip-coating process. The Nafion was purchased ready-made in a 5% dispersion. Due to limited availability (refer to environmental impact and sustainability) Nafion dispersions from two different manufacturers were used. Even though the brand names (Nafion D520 from Fisher Scientific and Nafion 117 from Sigma Aldrich) and the solvents stated in the safety datasheet (SDS) were slightly of different composition, it resulted in no observable optical or uniformity difference in the DBR stack. The original Nafion dispersion was too viscous and resulted in thicker layers than what was needed; thus, it was diluted with 2-propanol down to 3% dispersion, which was the case for both solutions.

3.1.2 PVA preparation

For high refractive index material TiOH was used in a PVA matrix. PVA is a water-soluble and widely used polymer in the glue industry. PVA was prepared by dissolving PVA in pure water in a 7.5g/L ratio. The PVA used was the Mowiol® 18-88 with a molecular weight of M_w=130,000 from Sigma Aldrich

3.1.3 Titanium hydroxide synthesis

The titanium hydroxide was synthesized directly in water by slowly hydrolyzing titanium chloride in a ratio of 2.2mL of $TiCl_4$ in 20mL of water. This is an intense exothermic reaction; thus, the whole solution was placed in an ice bath to control the temperature. The dripping was maintained at around one drop per 10s, which was done in order to allow the solution to cool down. It is worth noting that the $TiCl_4$ will produce hydrochloric acid both in solution and in vapor form. Thus,

the whole apparatus was placed inside a fume hood. The procedure was adopted by Russo et al [64]. Finally, to create the TiOH/PVA, the TiOH solution was combined with PVA at 50% [65]. The TiOH was obtained from Sigma Aldrich.

3.2 PVD of organic emitters and metal mirrors

TDAF is an organic semiconductor that emits light in the blue region [52]. TDAF can be deposited in solution (ref), but in this work, it was deposited using thermal deposition. The PVD system was used to evaporate the TDAF, lithium fluoride (LiF), and the aluminum mirror. The thermal deposition was used for the fabrication of hybrid microcavities, which were composed of a solution-processed DBR, the organic emitter/LiF, and finally, the metal mirror. Thus, we thermally evaporated 50nm of TDAF followed by 5nm of LiF and an 80nm aluminum mirror. The lithium fluoride was used in order to limit the diffusion of aluminum in the TDAF layer [66–68]. The deposition rates were 1 Å for TDAF, 0.2 Å for LiF, and 0.5 Å for aluminum. Finally, the deposition vacuum was $>8 \times 10^{-6}$

3.3 Substrates

The substrates that were used to fabricate the photonic devices were from quartz with dimensions 15mm by 15mm and 1mm thickness. Quartz substrates were used since they have well-documented characteristics and low surface roughness; in addition to that, they pose exceptional UV performance. Silicon substrates were used for thin film characterization for reasons similar to those of quartz substrates, mainly the thin Silicon Dioxide layer that is formed on the surface. All substrates were cleaned with a 3-step procedure, which consisted of 10-minute sonication in a 3% Decon90 detergent solution followed by acetone and, finally, IPA. In each step, the substrates were dipped in the next step's solution, which was discarded and replaced with a fresh one in order to minimize cross-contamination. After the last step, the

substrates were blow-dried using 99.999% N5 nitrogen gas and immediately used for deposition in order to minimize contamination from the environment. The fused silica substrates were purchased from APEX OPTICAL SERVICES.

3.4 Equipment

In this section, the essential equipment and measurement techniques used in this thesis will be described. Excluding the basic lab supplies and instruments such as pipettes, scales, and sonicators to maintain clarity, this section will focus on the more specialized equipment that is important for the research.

3.4.1 Physical vapor deposition

To produce neat films of materials such as metals, organics, and dielectrics, a precise and accurate deposition is required. Physical vapor deposition can deposit such materials with nanometer precision at a controlled deposition rate. A PVD system is a chamber that utilizes partial to high-vacuum in order to be able to evaporate materials. The PVD system can utilize different techniques in order to evaporate materials such as sputtering and thermal evaporation. The evaporator used is from Angstrom Engineering which has in total 9 deposition sources. The evaporator has two sputtering sources, 4 radak sources and 3 resistive/thermal sources. Sputtering is a technique where plasma is created from a high-frequency AC source inside a partial vacuum. The high-speed ions are bombarding the target material, which basically detaches molecules from the target and deposits them to the substrate. Evaporating deposition uses thermal energy in a high vacuum in order to evaporate or sublimate the material used. In this evaporator, two different types of thermal sources are used. The thermal evaporator sources use a resistive heater boat, which directly melts and evaporates the material and is power-controlled. Similarly, radak sources also use heat energy in order to evaporate the material, but instead of

directly heating the material, they use a heater element that indirectly heats the material, usually in an alumina boat. Radak sources are temperature-controlled, and they are suitable for temperature-sensitive materials like organics.

3.4.2 Dip-coater

For the dip-coating, an Ossila dip coater was used. The dip-coating is a very simple and straight forward technique where a substrate is lowered into a solution for a certain amount of time in order to wet the surface. Afterward, the substrate is retracted at a certain speed. Even though dip-coating is a very simple technique there are a lot of parameters that define the film thickness and generally the quality of the film [69, 70]. Because a DBR is a multi-layer structure there was a need to automate the procedure in order to avoid any human interference in the process. Thus, a straightforward yet effective automation was created that integrated the processes of solution switching and annealing into a single linear axis movement. The automation was developed in-house[71] using a repurposed CD/DVD laser head drive and an Arduino mini development board. This automation enabled the production of significantly higher-quality structures compared to the ones that were fabricated manually. The Dip-coater, along with the automation, can be seen in Figure 9.

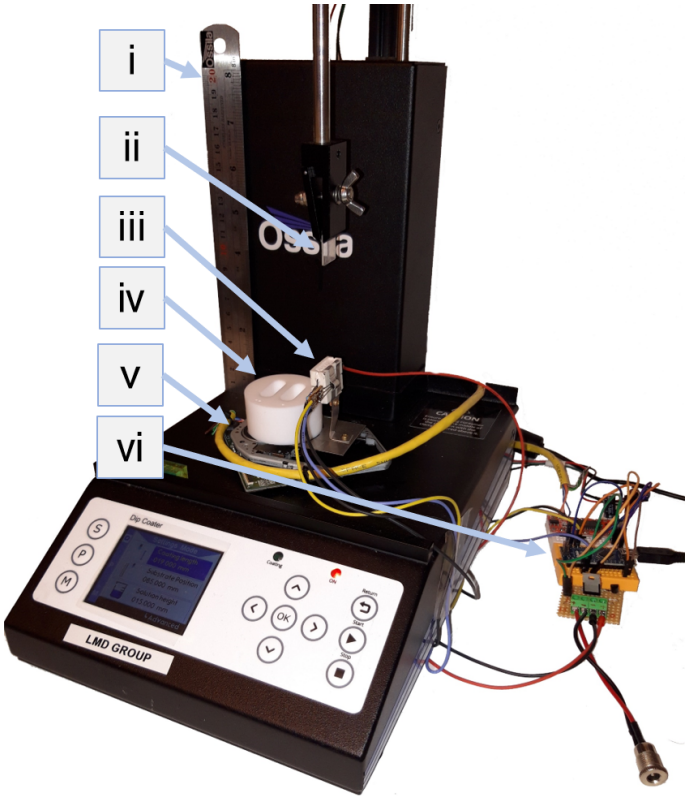

Figure 9. The Ossila dip-coater with the automation and its controlled electronics. i) Ossila dip-coater. ii) Quartz substrate along with its holder. iii) The PID-controlled heater element. iv) Solutions vessel. v) The step-motor controlled linear stage. vi) Microcontroller and supporting circuitry in order to control the automation process.

3.4.3 Transmission and angle-resolved measurements

The transmission of the samples was measured using a self-made in-house transmissivity setup seen in Figure 10. The setup consists of the Avalight-D(H)-S deuterium-halogen light source and an OceanOptics USB2000 spectrometer. The optical section of the setup was built from discrete components from ThorLabs. The light source was coupled to a fiber and the light output was collimated using a 50mm convex lens. After the collimation, the light dispersion was limited using an aperture to avoid errors due to chromatic aberration coming from the lens and the out-of-line emission between the deuterium and halogen lamp. Finally, the light passed through

the sample and then the transmitted light was collected and transferred with a fiber to the spectrometer. In order to properly measure the transmission of a sample, first a reference has to be measured by measuring a bare substrate. Afterwards, without changing any parameters we place the sample onto the holder. By taking a proper reference we can measure only the bare film without any interference from the substrate. In addition to that, the light source was left to warm up for at least 20 minutes before the measurement to avoid any fluctuations.

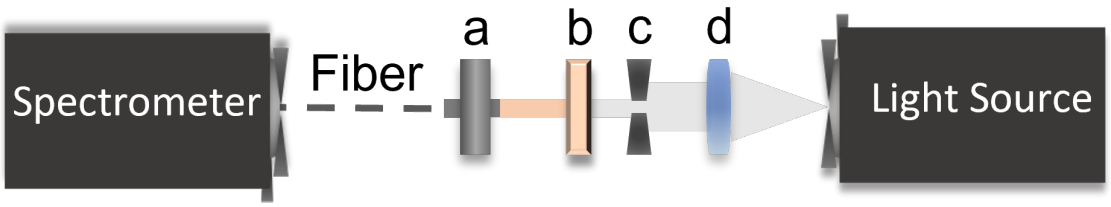

Figure 10. The in-house transmission setup is depicted. On the right, the deuterium-halogen light source is shown, which provides the light, and on the left, the spectrometer collects the transmitted light through the sample. a) This is the fiber coupler, which holds the fiber at a specific location going to the spectrometer. b) The holder in which the sample was fixed in place in order to be measured. c) An aperture that limits the dispersion of the collimated light. d) A 50mm focal length convex lens that collates the light coming from the fiber.

The angle-resolved reflectivity and photoluminescence measurement setup was also a custom-built setup. The optical/measurement setup was the same in both measurement techniques with the only difference being the light source and the excitation implementation. The measurement setup is composed of a 2-D spectrometer using the PIXIS 400 CCD camera and an optical path composed of two lenses, a beam splitter, and an objective. The objective, due to its large numerical aperture NA, can collect angles of around 40 °. In the angle-resolved reflectivity, a white light source illuminates the sample through a beam splitter and a collimation lens and finally passes through the objective to the sample. Afterward, the reflected image passes through the objective, through the beam splitter, through a collimation lens,

and finally to the spectrometer, where the 2-D image of the spectrum is projected to the camera seen in Figure 11. In the angle-resolved photoluminescence instead of the white light source, a laser source is used instead. Figure 11 depicts the setup and the light path.

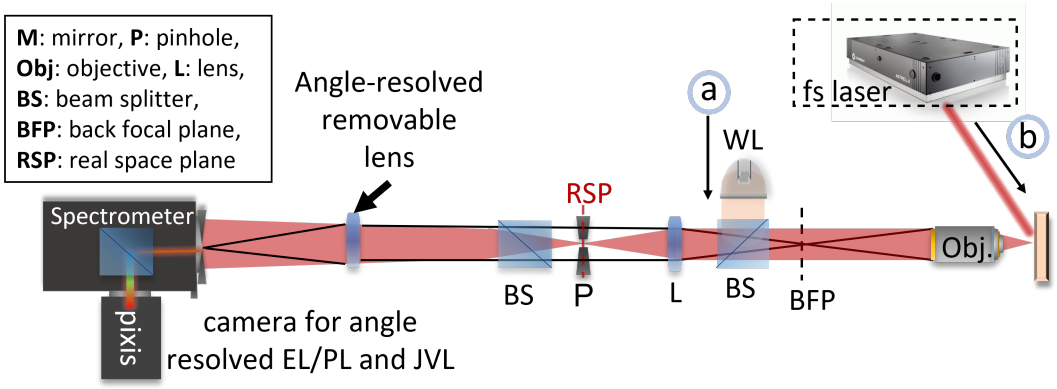

Figure 11. Schematics of the custom angle-resolved reflectivity and photoluminescence schematic is shown. The light path from the white light source is shown with yellow and the reflection/photoluminescence light path is shown with light blue. a) Light from the white light source. b) Laser beam for the photoluminescence measurements.

3.4.4 Ellipsometer

An ellipsometer is an optical instrument used to measure the properties of thin films. It works by analyzing the change in polarization as light reflects off a sample surface. When the polarized light hits the surface, can alter the polarization state, depending on the material's properties and the film thickness. The polarization state is the magnitude of the s and p polarized light. The s-and p-polarization is the magnitude of the reflected electric field perpendicular to the plane of incidence for s and in the plane of incidence for p. With the information of amplitude between s and p over time we can extract the Δ and Ψ values. The Δ is the phase difference between the s- and p-polarized light that is reflected after the sample. The Ψ is the amplitude ratio between the s-and p-polarized light that is reflected after the sample. Graphing the s and p can result in a straight line up to a perfect circle, usually though it is an ellipse, from which the name of the ellipsometer is derived. By measuring these changes, an ellipsometer can determine the film's thickness, refractive index, and extinction coefficient. These measurements are crucial in various fields, such as semiconductor manufacturing, where precise control over thin film properties is essential for device performance. The technique is nondestructive, and, in this work, it played a crucial role in characterizing our films in order to improve our TMM simulations. Furthermore, with the ellipsometer, we measured the dispersion of the cavity and polariton states along with the angle–resolved spectroscopy. The ellipsometer that we used is the VASE ellipsometer from J.A Woollam is seen in the figure below.

Figure 12. The VASE ellipsometer used to measure the film parameters along with the dispersion and polariton states [72].

4 Results

The optimization of the solution concentration and preparation was done by Emilia Palo. Even though this optimization produced excellent single-layer films, the procedure fell short of producing a uniform, non-diffusive DBR. For the realization of DBRs capable of producing high-Q microcavities, significant engineering, and additional optimization procedures had to be realized. Procedures included a strict cleaning protocol and fresh solutions for each deposition. Nevertheless, by far the most significant improvement was the engineering of the automated dip-coating setup. In this section, all the necessary and crucial results will be presented.

4.1 Nafion and PVA optimization film characterization

A DBR needs to have a precise and well-defined stopband, both in terms of amplitude and in terms of wavelength. Thus, careful characterization of the bare thin-film materials is needed, in order to be able to calculate the proper thicknesses and amount of layers to achieve the desired results. In order to be able to calculate the DBR parameters, the refractive index of the material and the absorption coefficients need to be known. In a PVD system, the films can be deposited very precisely, but when dealt with solution-processable techniques, a lot of challenges emerge. First and foremost, the deposition thickness needs to be extremely precise, which is challenging in solution-processable approaches due to the many parameters that affect it. A proper evaluation needs to be done on how and what parameters affect the thickness the most.

In order to minimize the variables, the dip-coater retraction and protraction rate were kept constant. The thickness was primarily affected by the solution viscosity and the annealing parameters. The solution viscosity can be easily controlled by the ratio of solvents in the solution. The annealing parameters involve the annealing temperature and annealing time. The combination of these annealing parameters

affects the film thickness and the refractive index change. Fully characterizing these parameters is crucial in order to understand the behavior of the material and choose the parameters that maximize the refractive index contrast, minimize the deposition time, and find the appropriate annealing temperature. The annealing temperature is needed in order to evaporate the solvents trapped in the polymers. The deposition time needs to be minimized for two reasons: the overall speed of fabrication and limiting the evaporation of the solutions, which can affect the deposition thickness.

The low refractive index material (Nafion) and the high refractive index material (PVA/TiOH) were deposited with different concentrations and then their film properties were measured with an ellipsometer at 500nm shown in figure 13. Nafion showed an almost perfect linear response with its concentration, rendering the deposition thickness easy to calculate as shown in figure 13a. Heating the Nafion occurred at 90°C for 1 minute. The thickness barely changed with the temperature and the small difference can be considered an error. Nafion also showed a very stable refractive index which was unaffected by any change in parameters. The PVA/TiOH was a bit more challenging. The thickness showed a linear response with the concentration when the film was not annealed. After annealing the thickness reduced substantially. The PVA/TiOH is dissolved in water. Thus, this reduction in thickness is attributed to the swell of the PVA matrix with the water; drying removes the trapped water, which reduces the thickness as shown in figure 13b. The most notable change (figure 13c) was the refractive index change with and without annealing with the former showing a substantial increase. Thus, for the PVA/TiOH the concentration and annealing affected the optical thickness of the material.

After the thickness optimization, a full spectrum ellipsometer characterization was conducted in order to be able to model the refractive index change and to calculate the optical thicknesses in terms of wavelength. As it is shown in figure 13d, Nafion has a textbook refractive index response with no absorption even in the

UV region. The case was not the same with the PVA/TiOH. Here the absorption increased significantly after around 375nm due to the TiOH. Nevertheless, the material choice proved to be sufficient in order to produce a stopband in the UV-blue region where the TDAF absorption is.

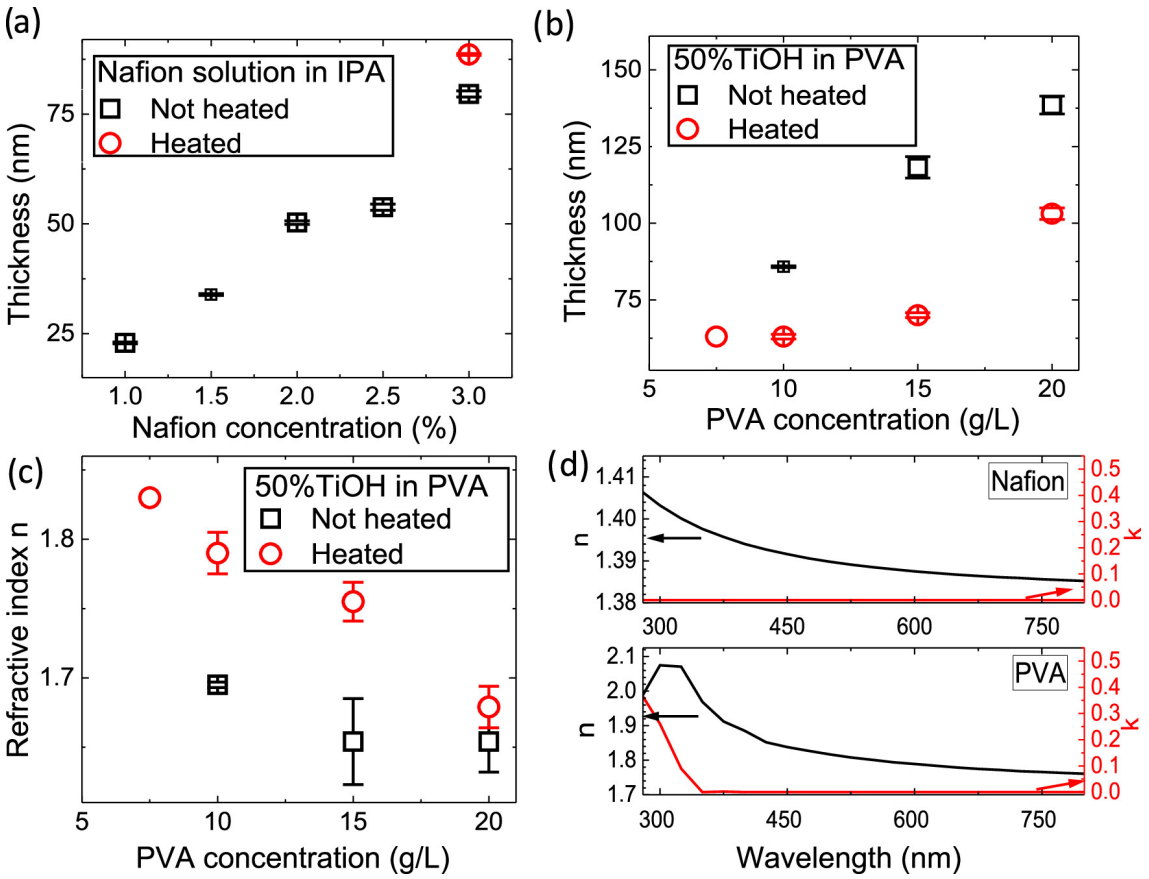

Figure 13. The optimization results for the ellipsometer are shown. The measurements of a,b, and c figures took place at 500nm a) The Nafion thickness increased with the concentration in a linear fashion. Heating the film, a minuscule increase in thickness can be observed, which was in the range of error. b) The PVA/TiOH thickness relative to the solution concentration. Before heating, a linear increase of the thickness is observed, while after heating, the thickness is reduced and increased in an exponential fashion. c) The refractive index of PVA/TiOH is shown. The refractive index increased substantially after heating and reduced with the increase in concentration. d) The refractive index n and extinction coefficient k are shown at the full spectrum. PVA/TiOH shows a significant absorption in the UV region while Nafion showed no absorption in the full spectrum.

The PVA/TiOH posed a different problem which the Nafion lacked. Further film

characterization with the ellipsometer revealed a significant depolarization increase *(figure 14)* between a new solution and an old solution which indicated scattering in the film. This was attributed to the aggregation of TiO_2 which was formed from the TiOH. Thus, for good performing DBR it was very important to start the depositions with fresh solutions.

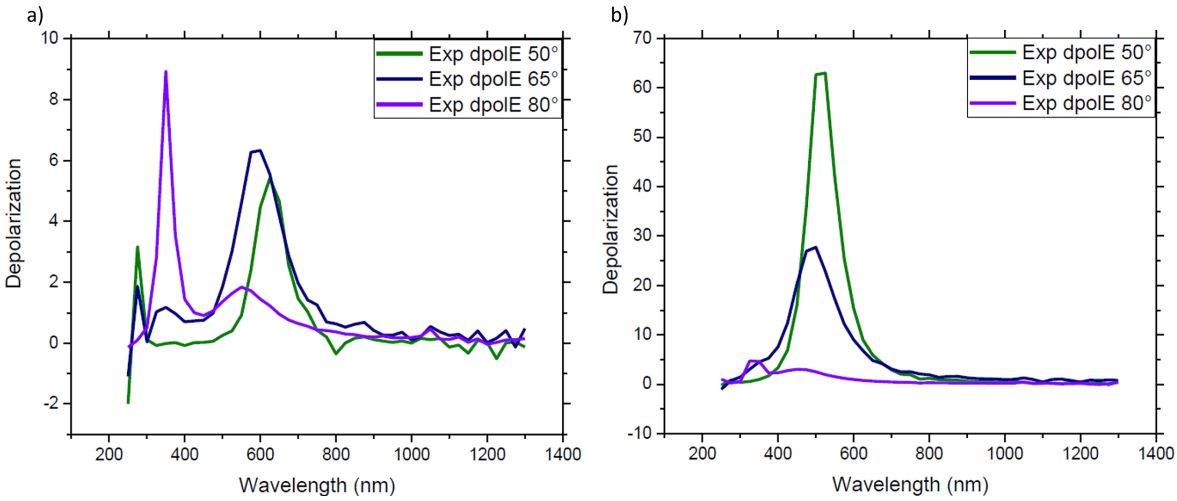

Figure 14. The depolarization of PVA/TiOH film is shown. a) This film was made with a fresh solution. A minuscule depolarization can be observed. b) This film was made with a day old solution. A significant depolarization can be seen indicating scattering. This was attributed to the formation of aggregations in the solution.

4.2 DBR characterization

After the Nafion and PVA/TiOH single film characterization, the film thicknesses could be calculated and a DBR can be developed. While fabricating the DBR, extreme caution was applied in cleanliness in order to reduce the likelihood of contamination. The deposition parameters are described in detail in the experimental, section 3.1. The DBRs were characterized mainly using the transmission setup. In the figure 15 a final DBR can be seen along with its transmission. It can be observed that the DBR shows excellent coverage for a dip-coating procedure, while some non-uniformity at the edges is to be expected due to the surface tension. The

stopband of the DBR is well defined with excellent reflectivity of >90% . Furthermore, the stopband exhibits an insignificant shift to most of the DBR area except near the edges where the thickness is non-uniform. The DBR structure included 6 pairs, balancing reflectivity and speed. Adding more pairs wouldn't necessarily improve reflectivity because of minor absorption and scattering within the layers. For example, 8-pairs might have resulted in worse reflectivity due to the film absorption.

The transmission spectra indicates a capable DBR for the use in polariton research, with controllable stopband and reflectivity. More importantly this was done automatically by the dip-coater thus, no-human intervention was needed resulting in increased productivity and quality.

Another important parameter is the lifetime of the DBR. Thus, a DBR was measured at the same spot after 4 months. No observable stopband shift was found, and most importantly, no reduction in transmission. Thus, there was no indication of DBR degradation. In the figure 16 the initial and the aged spectra can be seen with a small reduction in the Bragg modes attributed to the error in the measurement.

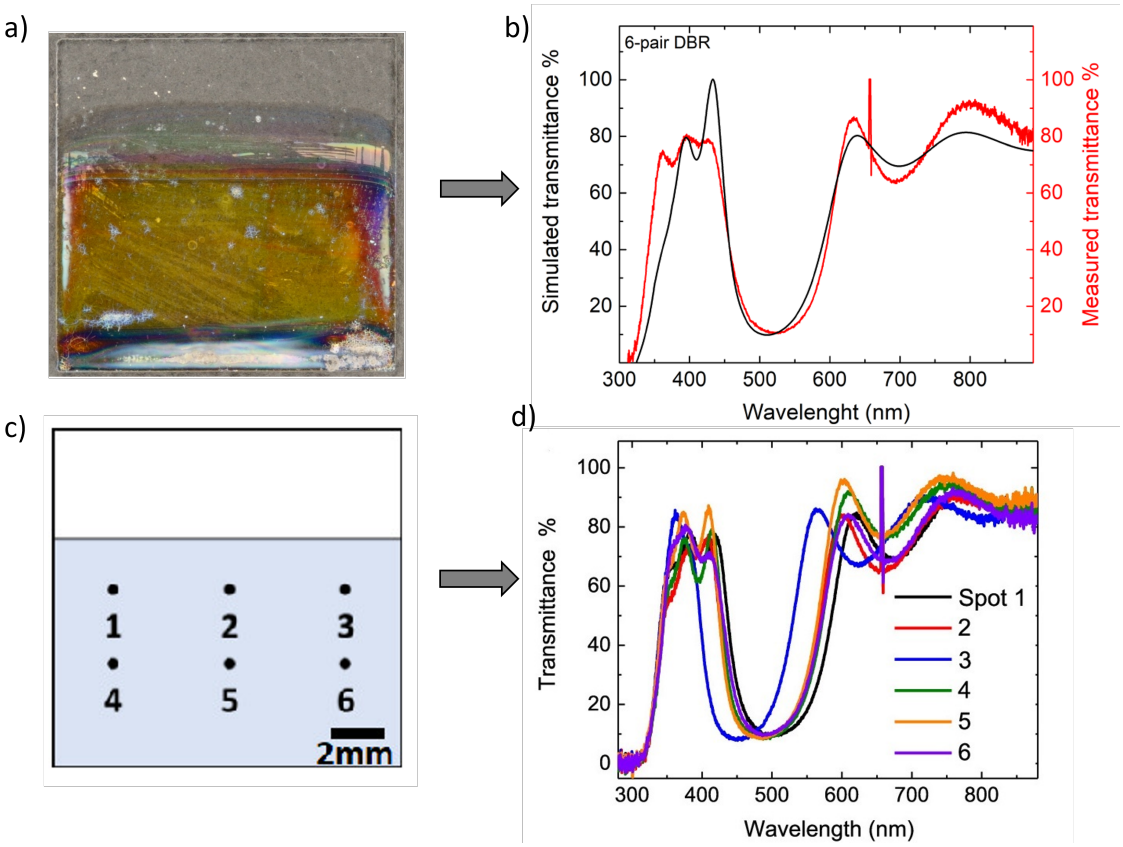

Figure 15. a) A photo of a solution-processed DBR which shows excellent coverage and uniformity taking into account that it was made from a simple dip-coating process. b) The transmittance spectra of the same sample exhibiting an excellent <10% transmittance. Furthermore, a simulation is shown which confirms the accuracy of the experimental setup.

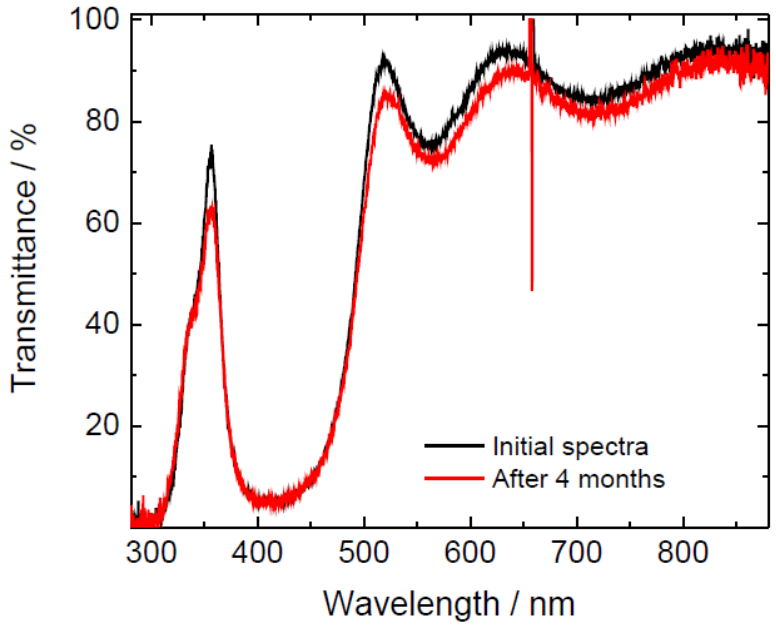

Figure 16. The spectra of a fresh device and an aged DBR. As it can be seen no meaningful distinction of the stopband can be made.

4.3 Empty monolithic microcavity

Having fully characterized the DBRs, the next step is to fabricate a full solution-processed empty microcavity. With a small modification of the software, the automation allowed the realization of such microcavity. The microcavity consists of two DBR mirrors with a spacer in between. The spacer was fabricated by double-dipping the sample in the PVA/TiOH solution. As mentioned in the section 2.3 for a single order microcavity the length should be of $\lambda/2 \cdot n$ whereas the single layer thickness of a DBR is $\lambda/4 \cdot n$. It is immediately obvious that the double dipping will create the desired thickness without the need for an additional step and a separate solution. The PVA dissolves slowly enough to allow for such double dipping without any significant reduction in thickness. A schematic representation of the cavity is shown in the figure 17.

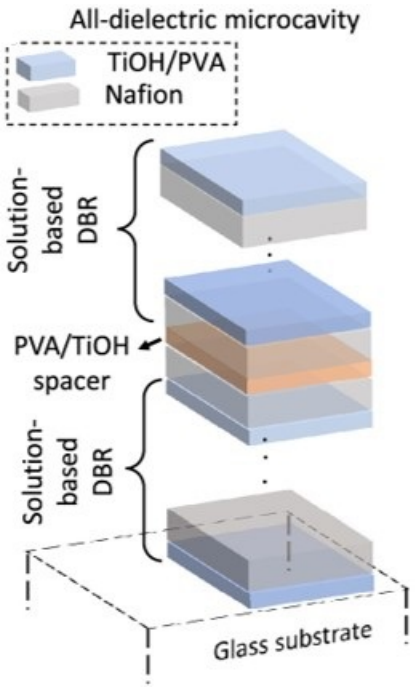

Figure 17. The schematic structure the empty microcavity. The PVA/TiOH spacer was deposited the dual dipping in the PVA/TiOH solution.

The cavity consisted of a total of 26 layers, which is at the limit of our method

at the current settings. As it can be seen from the figure 18, the edges of the sample exhibit significant inhomogeneity, which is expected. Due to the small size of the substrate, the thickness of the inhomogeneous part was a couple of millimeters. Nevertheless, there was a significant area at the center of the device in which a full microcavity had been developed. As it can be seen in figure 18, the Q-factor has an exceptional value of 91, which is among the highest reported values than the currently known sub-10 DBR pairs microcavity[46, 47]. This proves the concept of a capable microcavity for polaritonic applications.

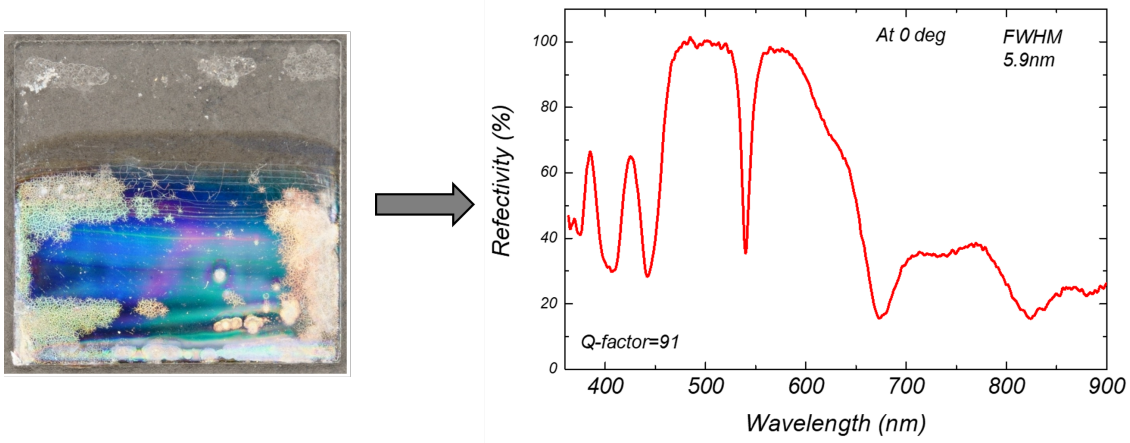

Figure 18. On the left a photo of the empty microcavity is shown. On the right, the reflectivity is shown where a full-width half maximum (FWHM) of 5.9nm and a Q-factor of 91 can be seen. This indicated a capable microcavity for polaritons.

In order to fully characterize the fully dielectric microcavity, an angle-resolved reflectivity was conducted with the ellipsometer. In figure 21, the cavity mode can be observed along with the Bragg modes in both s (transverse magnetic) and p (transverse electric) polarizations. This concludes the characterization of the empty/fully dielectric microcavity, which shows an excellent cavity mode for a fully solution-processed fabrication at only 6 DBR pairs.

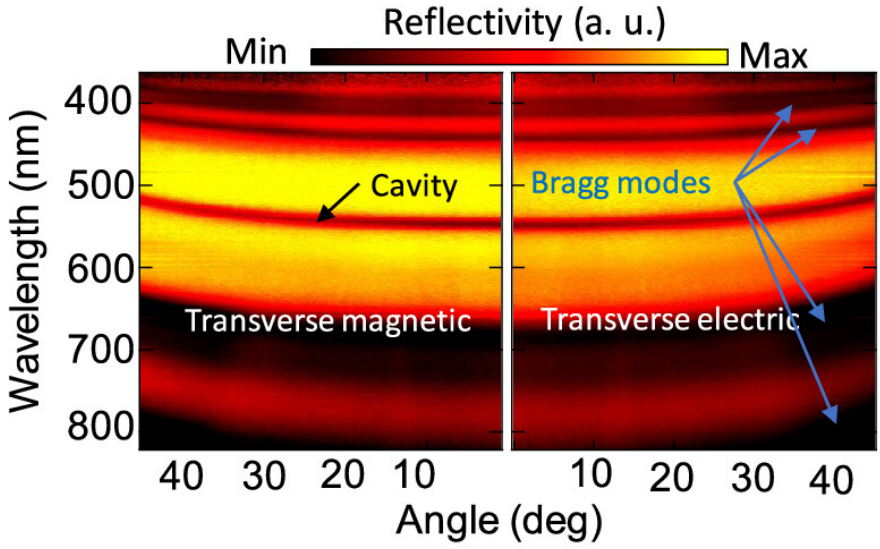

Figure 19. The angle-resolved reflectivity. The cavity mode be clearly seen along with the Bragg modes. The measurement was conducted with the ellipsometer in both transverse magnetic and transverse electric.

4.4 Hybrid polariton microcavity

Despite the substantial progress and advancements in fabricating a fully processable DBR and an empty microcavity, creating a full solution-processable polaritonic microcavity was fruitless. This accounts for many factors but mainly due to incompatibilities in the solvents of the TDAF organic excitonic emitter. Driven by motivation and scientific curiosity, it was still important to prove that a solution-processed by DBR was of such quality that can induce polaritons in a microcavity. Thus, we fabricated a hybrid microcavity. The microcavity was fabricated with the first mirror being a solution-processed DBR followed by the thermal deposition of TDAF and finally a thermal deposition of an aluminum mirror as illustrated in the figure 20.

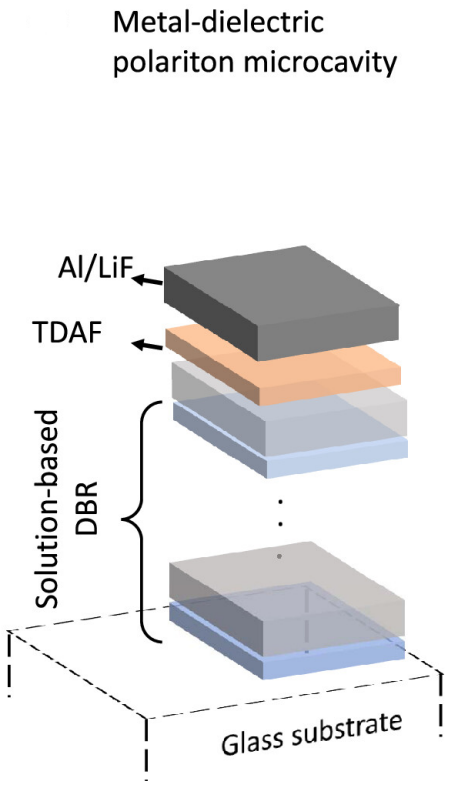

Figure 20. The schematic structure of the hybrid-microcavity. The microcavity consists of a dip-coated DBR, a thermally evaporated organic emitter (TDAF), and an aluminum mirror.

From the figure 21 and using the k-space reflectivity setup, it is shown that the lower polariton was clearly shown. This proves the capability of the solution-processable DBRs. This work, in particular, was especially challenging due to the absorption of TDAF being in the near-UV region. Thus, the upper polariton was not clearly visible due to the strong absorption of the TiOH. Nevertheless, it is shown that even in these challenging parameters, the hybrid design and fabrication were able to exhibit polaritons in the TDAF emitter.

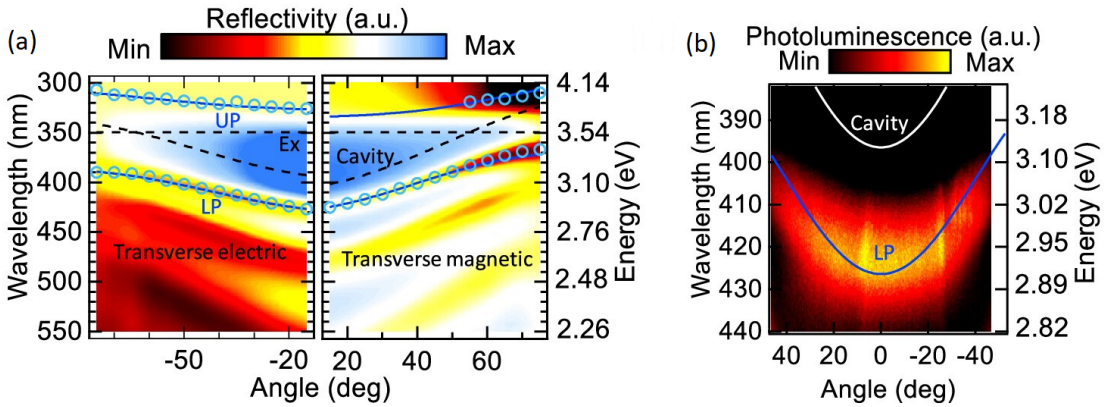

Figure 21. The angle-resolved reflectivity and photoluminescence. The device in the k-space photoluminescent setup was excited with a 375nm 250fs laser pulse at 200kHz repetition rate. a) The reflectivity in the transverse electric and magnetic polarization. The blue circles indicate the polariton minima whereas. These minima where utilized in the simulation where it is shown with the blue solid line., where the uncoupled exciton along with the cavity mode is shown with the black dashed line. b) The angle-resolved k-space photoluminescence is shown where the lower polariton is shown with the blue line and the cavity mode with the white line.

The Rabi splitting Ω between the LP and UP was obtained by fitting a coupled harmonic oscillator model to the reflectivity spectra shown in figure 22. The fitting is in perfect agreement with the measurements. Furthermore, the fitting is also in agreement with literature [26, 73]. The Rabi splitting of Ω 803meV for the transverse-magnetic was obtained with a cavity detuning of -402meV and a n_{eff} of 1.9. For the transverse-electric, the Rabo splitting was of Ω 750meV with n_{eff} of 1.6. The smaller Rabi splitting in the latter case is attributed to the limitation in our simulation model (refer to: 4.5) and the low contrast of the UP due to the absorption of the DBR at the higher wavelengths. Finally, a different microcavity is shown with a different detuning of -320meV.

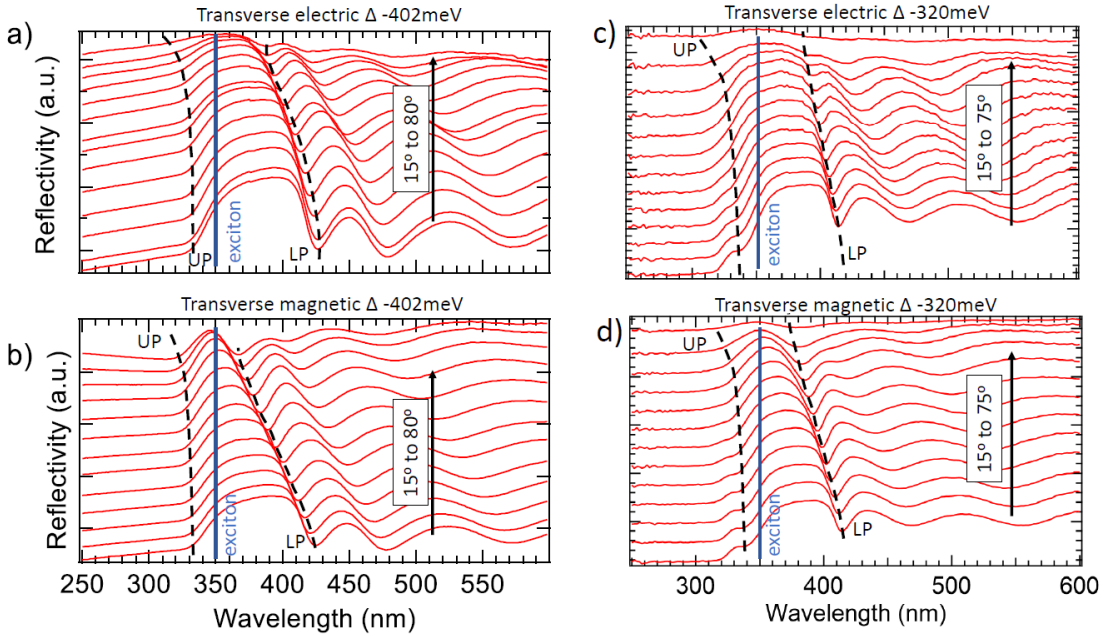

Figure 22. The reflectivity spectra obtained with the ellipsometer. These graphs provide a clear insight into the LP compared to the figure 21 a),b) Transverse electric and transverse magnetic for a microcavity with -402meV detuning. The solid blue line indicates the exciton, whereas the dashed lines indicate the UP and LP. c),d) Transverse electric and transverse magnetic for a microcavity with -320meV detuning. The solid blue line indicates the exciton, whereas the dashed lines indicate the UP and LP.

4.5 Simulations

To be able to test our designs and to check that our experimental measurements are accurate, we needed to be able to conduct accurate simulations of the DBRs and microcavities. Initial simulations were done using a modified Matlab code [74]. These initial simulations were proven inaccurate, and this was mainly attributed to the lack of an ellipsometer system at that time. Thus, limited data were obtained from 3rd party ellipsometer setup measurements at fixed 500nm wavelength [75]. After the acquisition of the ellipsometer the simulations were improved and proven to be very accurate, giving us an insight of the structure and how the layers behave in a stack. Such simulation is shown and compared in the figures 15 and 22. The model utilized a coupled-harmonic oscillator using the transfer matrix method. Although

the results were accurate and were predicting our measurements correctly, the model came with some limitations. For example, the model did not account for the angle-dependent penetration depth of the top DBR. The inconsistency in the simulation in the transverse electric of the first cavity is attributed to these limitations (figure 22).

5 Environmental impact and sustainability

In recent years, due to environmental changes and pollution, significant attention and research have been drawn in order to reduce waste and direct or indirect pollution. Thus, in this work, the author felt obligated to highlight the importance of their environmental impact and the steps they took to reduce it as much as possible. In addition to that, because of the rapid growth and the nature of this research field, it was impossible to precisely conduct environmental and energy impact for this research. Furthermore, conducting such research was outside of the scope of this work. Lastly, it is anticipated that this work will enable research in polaritons, which are believed to be the key to realizing OLEDs, which will lead to the realization of practical OLEDs for general illumination. Nevertheless, a concise overview will be described.

5.1 Energy consumption

The direct energy used for this research was mainly in the form of electricity. Energy usage came from normal usage of the lab equipment such as glovebox, ice maker, laser, characterization, etc. This amount of energy forms our baseline which was inevitably used throughout this work. Unfortunately, there are no precise measurements but an estimation can be based on the power consumption of each device and the utilization factor. Thus, the baseline power is grossly estimated to be $\approx$1kW average.

In this work solution processed DBRs replaced the conventional DBRs made from PVD. This alone contributes to significant energy savings since the highest energy-consuming device is the PVD. PVD is a time and energy-intensive process; thus, in order to fabricate a DBR using PVD, the energy of many kWh is required. In contrast, the dip-coater paired with the automation consumes energy in the order of Wh[76].

5.2 Fluoropolymers and forever chemicals

Nafion is a fluoropolymer that is used in this work as a low refractive index layer for the DBRs. Nafion is an exceptional material for this application due to its low refractive index and chemical stability. Even though Nafion has moderate toxicity, it has been shown that it and its derivatives are present in detectable amounts in drinking water. Furthermore, it has been shown that exposure to these chemicals negatively impacts rat birth rates.[77] Furthermore, Nafion and other fluoropolymers contribute to Per- and polyfluoroalkyl substances (PFAS) pollution.

PFAS are considered to be forever chemicals due to their extremely low reactivity and high resiliency. Forever chemicals are chemicals that are shown to be present in the environment in measurable quantities. They stay in the environment because no mechanism to break them down exists in nature. Thus, more research is needed in order to find a suitable replacement for Nafion in order to ease the environmental impact of this research. Lastly, the European Union is trying to phase out PFAS by strictly regulating their use and production. At the point of writing, there is a strong push in the European Union in order to completely ban PFAS[78].

5.3 Upcycling

It is worth mentioning that at the start of this research, it was immediately obvious that automation was needed in order to be able to achieve high-quality and repeatable results. It was recognized that a linear stage was needed and a heater in order to be able to control the deposition. Thus, instead of purchasing either a new automated dip-coater or building a brand new automation from preexisting materials, we turned our interest to reusing discarded materials from the department. Thus, an idea occurred to reuse an old CD/DVD drive in order to develop the automation needed. Thus, we upcycled electronic equipment meant for recycling into something useful.

6 Conclusions

In the organic semiconductors and the OLED world, research on how to improve device performance is crucial to the commercialization of these products. Furthermore, due to ever-increasing concern about the environment and the energy used to produce light-emitting devices, it is even more important to achieve the most efficient devices physics allows. One way to tackle these limitations is through photonics and optical and quantum engineering. DBRs are photonic structures that can improve the efficiency of a device through Purcell enchantment or through polaritons. In addition to that, DBRs can also improve outcoupling, improving the efficiency of a device. Even though the DBRs are promising, they are usually fabricated with a PVD system, which is time-consuming to fabricate DBRs, expensive, and very energy intensive. Thus, in the first part of this thesis, a solution-processable DBR is shown with excellent reflectivity/transmissivity, which was composed of Nafion as a low refractive index material and PVA/TiOH as a high refractive index material. In order to achieve these results we engineered and modified a linear stage with an integrated heater for annealing in order to fully automate the DBR production. This allowed for DBRs of an exceptional quality keeping in mind the dip-coating technique. Afterward, having established the procedure, we proceeded to fabricate a full solution-processed dielectric microcavity. This microcavity showed an impressive Q-factor of >91 which is on par or even better with a metallic microcavity. The next and final step is to create a microcavity with an organic emitter in order to prove the formation of polaritons. Due to solvent incompatibilities, it was unfeasible to fabricate a fully processable, fully dielectric microcavity with an organic emitter. Thus, in order to prove that the solution-processable DBRs are capable reflectors, we fabricated a hybrid dielectric-metal microcavity. This microcavity is composed of a solution-processed DBR reflector, a TDAF emitter, and finally, an aluminum mirror. TDAF emitter is a very challenging material for the solution-processable

DBRs due to the absorption of the TiOH in the near-UV region that the TDAF absorbs. Nevertheless, with this setup, and by conducting reflectivity and electroluminescent measurements we managed to show polaritons. This paves the way for affordable research in photonics in order to improve OLED devices.

References

[1] Raphael F. Ribeiro et al. "Polariton chemistry: controlling molecular dynamics with optical cavities". In: *Chemical Science* 9 (30 2018), pp. 6325–6339. ISSN: 20416539. DOI: 10.1039/c8sc01043a.

[2] Arkajit Mandal et al. "Theoretical Advances in Polariton Chemistry and Molecular Cavity Quantum Electrodynamics". In: *Chemical Reviews* 123 (16 Aug. 2023), pp. 9786–9879. ISSN: 15206890. DOI: 10.1021/acs.chemrev.2c00855.

[3] Sindhana Pannir-Sivajothi et al. "Driving chemical reactions with polariton condensates". In: *Nature Communications* 13 (1 Dec. 2022). ISSN: 20411723. DOI: 10.1038/s41467-022-29290-9.

[4] Sanjib Ghosh and Timothy C.H. Liew. "Quantum computing with exciton-polariton condensates". In: *npj Quantum Information* 6 (1 Dec. 2020). ISSN: 20566387. DOI: 10.1038/s41534-020-0244-x.

[5] Kavokin A. Liew T.C.H. Schneider C. et al. "Polariton condensates for classical and quantum computing". In: *Nature Reviews physics* ().

[6] Christopher R. Gubbin, Simone De Liberato, and Thomas G. Folland. "Surface phonon polaritons for infrared optoelectronics". In: *Journal of Applied Physics* 131 (3 Jan. 2022). ISSN: 10897550. DOI: 10.1063/5.0064234.

[7] Clàudia Climent et al. "Not dark yet for strong light-matter coupling to accelerate singlet fission dynamics". In: *Cell Reports Physical Science* 3 (4 Apr. 2022). ISSN: 26663864. DOI: 10.1016/j.xcrp.2022.100841.

[8] Raj Pandya et al. "Tuning the Coherent Propagation of Organic Exciton-Polaritons through Dark State Delocalization". In: *Advanced Science* 9 (18 June 2022). ISSN: 21983844. DOI: 10.1002/advs.202105569.

[9] Mao Wang, Manuel Hertzog, and Karl Börjesson. "Polariton-assisted excitation energy channeling in organic heterojunctions". In: *Nature Communications* 12 (1 Dec. 2021). ISSN: 20411723. DOI: 10.1038/s41467-021-22183-3.

[10] Kyriacos Georgiou et al. "Ultralong-Range Polariton-Assisted Energy Transfer in Organic Microcavities". In: *Angewandte Chemie - International Edition* 60 (30 July 2021), pp. 16661–16667. ISSN: 15213773. DOI: 10.1002/anie.202105442.

[11] Anton Matthijs Berghuis et al. "Enhanced Delayed Fluorescence in Tetracene Crystals by Strong Light-Matter Coupling". In: *Advanced Functional Materials* 29 (36 Sept. 2019). ISSN: 16163028. DOI: 10.1002/adfm.201901317.

[12] Vasileios C. Nikolis et al. "Strong light-matter coupling for reduced photon energy losses in organic photovoltaics". In: *Nature Communications* 10 (1 Dec. 2019). ISSN: 20411723. DOI: 10.1038/s41467-019-11717-5.

[13] Xiaolan Zhong et al. "Non-Radiative Energy Transfer Mediated by Hybrid Light-Matter States". In: *Angewandte Chemie* 128 (21 May 2016), pp. 6310–6314. ISSN: 0044-8249. DOI: 10.1002/ange.201600428.

[14] Emre Togan et al. “Polariton Electric-Field Sensor”. In: *Physical Review Letters* 125 (6 Aug. 2020). ISSN: 10797114. DOI: 10.1103/PhysRevLett.125.067402.

[15] Ignacio Vitoria et al. “Surface exciton plasmon resonances (SEPR)–based sensors”. In: *Optics and Lasers in Engineering* 160 (Jan. 2023). ISSN: 01438166. DOI: 10.1016/j.optlaseng.2022.107273.

[16] Shereena Joseph, Swagato Sarkar, and Joby Joseph. “Grating-Coupled Surface Plasmon-Polariton Sensing at a Flat Metal-Analyte Interface in a Hybrid-Configuration”. In: *ACS applied materials interfaces* 12 (41 Oct. 2020), pp. 46519–46529. ISSN: 19448252. DOI: 10.1021/acsami.0c12525.

[17] P I Nilutln and A A Beloglazov. *A multi-purpose sensor based on surface plasmon polaron resonance in a Schottky structure*. 1994.

[18] Weifang Yang et al. “High sensitivity gas sensor based on surface exciton polariton enhanced photonic spin Hall effect”. In: *Optics Express* 31 (16 July 2023), p. 27041. ISSN: 10944087. DOI: 10.1364/oe.497262.

[19] Ivana Podunavac et al. “Microwave spoof surface plasmon polariton-based sensor for ultrasensitive detection of liquid analyte dielectric constant”. In: *Sensors* 21 (16 Aug. 2021). ISSN: 14248220. DOI: 10.3390/s21165477.

[20] Denis A. Sannikov et al. “Room temperature, cascadable, all-optical polariton universal gates”. In: *Nature Communications* 15 (1 Dec. 2024). ISSN: 20411723. DOI: 10.1038/s41467-024-49690-3.

[21] Tony Mathew Blessan, C. Venkateswaran, and N. Yogesh. “All-optical terahertz logic gates based on coupled surface plasmon polariton sub-wavelength waveguiding in bulk Dirac semimetal”. In: *Optik* 257 (May 2022). ISSN: 00304026. DOI: 10.1016/j.ijleo.2022.168795.

[22] M A Baldo et al. *Highly efficient phosphorescent emission from organic electroluminescent devices*. 1998.

[23] Malte C. Gather, Anne Köhnen, and Klaus Meerholz. *White organic light-emitting diodes*. Jan. 2011. DOI: 10.1002/adma.201002636.

[24] S. Kéna-Cohen and S. R. Forrest. “Room-temperature polariton lasing in an organic single-crystal microcavity”. In: *Nature Photonics* 4 (6 June 2010), pp. 371–375. ISSN: 17494885. DOI: 10.1038/nphoton.2010.86.

[25] Johannes D. Plumhof et al. “Room-temperature Bose-Einstein condensation of cavity exciton-polaritons in a polymer”. In: *Nature Materials* 13 (3 Mar. 2014), pp. 247–252. ISSN: 14761122. DOI: 10.1038/nmat3825.

[26] K. S. Daskalakis et al. “Nonlinear interactions in an organic polariton condensate”. In: *Nature Materials* 13 (3 2014), pp. 271–278. ISSN: 14764660. DOI: 10.1038/nmat3874.

[27] Sai Kiran Rajendran et al. “Low Threshold Polariton Lasing from a Solution-Processed Organic Semiconductor in a Planar Microcavity”. In: *Advanced Optical Materials* 7 (12 June 2019). ISSN: 21951071. DOI: 10.1002/adom.201801791.

[28] Armando Genco et al. “Bright Polariton Coumarin-Based OLEDs Operating in the Ultrastrong Coupling Regime”. In: *Advanced Optical Materials* 6 (17 Sept. 2018). ISSN: 21951071. DOI: 10.1002/adom.201800364.

[29] Julia Witt et al. “High-Brightness Blue Polariton Organic Light-Emitting Diodes”. In: *ACS Photonics* 11 (5 May 2024), pp. 1844–1850. ISSN: 23304022. DOI: 10.1021/acsphotonics.3c01610.

[30] Hongyu Yang et al. “Ultralow Threshold Room Temperature Polariton Condensation in Colloidal CdSe/CdS Core/Shell Nanoplatelets”. In: *Advanced Science* 9 (18 June 2022). ISSN: 21983844. DOI: 10.1002/advs.202200395.

[31] Andreas Mischok et al. “Highly efficient polaritonic light-emitting diodes with angle-independent narrowband emission”. In: *Nature Photonics* 17 (5 May 2023), pp. 393–400. ISSN: 17494893. DOI: 10.1038/s41566-023-01164-6.

[32] Yu Bai et al. “Outcoupling of trapped optical modes in organic light-emitting devices with one-step fabricated periodic corrugation by laser ablation”. In: *Organic Electronics* 12 (11 2011), pp. 1927–1935. ISSN: 15661199. DOI: 10.1016/j.orgel.2011.08.004.

[33] Guorui Zhang et al. “Enlarging the Purcell Enhancement by Inserting a Dielectric Film in Dielectric-Loaded Surface-Plasmon-Polariton Waveguides”. In: *Advanced Quantum Technologies* 3 (9 Sept. 2020). ISSN: 25119044. DOI: 10.1002/qute.202000033.

[34] Hideo Iwase, Dirk Englund, and Jelena Vučković. *Analysis of the Purcell effect in photonic and plasmonic crystals with losses*. 2010. URL: http://www.stanford.edu/group/nqp.

[35] F. Hu et al. “Imaging exciton-polariton transport in MoSe 2 waveguides”. In: *Nature Photonics* 11 (6 June 2017), pp. 356–360. ISSN: 17494893. DOI: 10.1038/nphoton.2017.65.

[36] Fengsheng Sun et al. “Polariton waveguide modes in two-dimensional van der Waals crystals: An analytical model and correlative nano-imaging”. In: *Nanoscale* 13 (9 Mar. 2021), pp. 4845–4854. ISSN: 20403372. DOI: 10.1039/d0nr07372e.

[37] P. M. Walker et al. “Ultra-low-power hybrid light-matter solitons”. In: *Nature Communications* 6 (Sept. 2015). ISSN: 20411723. DOI: 10.1038/ncomms9317.

[38] Paul M. Walker et al. “Spatiotemporal continuum generation in polariton waveguides”. In: *Light: Science and Applications* 8 (1 Dec. 2019). ISSN: 20477538. DOI: 10.1038/s41377-019-0120-7.

[39] T. P. Rasmussen et al. “Polaritons in Two-Dimensional Parabolic Waveguides”. In: *ACS Photonics* 8 (6 June 2021), pp. 1840–1846. ISSN: 23304022. DOI: 10.1021/acsphotonics.1c00481.

[40] Chinmaya Kar et al. *Tamm plasmon polariton in planar structures: A brief overview and applications*. Apr. 2023. DOI: 10.1016/j.optlastec.2022.108928.

[41] Kazma Komatsu et al. "Few-Cycle Surface Plasmon Polaritons". In: *Nano Letters* 24 (8 Feb. 2024), pp. 2637–2642. ISSN: 15306992. DOI: 10.1021/acs.nanolett.3c04991.

[42] Israel De Leon, Pierre Berini, and D J Bergman. *Surface plasmon subwavelength optics*. 1988.

[43] Yasser Fuentes-Edfuf et al. "Surface Plasmon Polaritons on Rough Metal Surfaces: Role in the Formation of Laser-Induced Periodic Surface Structures". In: *ACS Omega* 4 (4 Apr. 2019), pp. 6939–6946. ISSN: 24701343. DOI: 10.1021/acsomega.9b00546.

[44] Lei Zheng et al. "Experimental demonstration of surface plasmon polaritons reflection and transmission effects". In: *Sensors (Switzerland)* 19 (21 Nov. 2019). ISSN: 14248220. DOI: 10.3390/s19214633.

[45] R J Nicholas. *SERIES ON SEMICONDUCTOR SCIENCE AND TECHNOLOGY Series Editors*.

[46] Giovanni Manfredi et al. "Directional Fluorescence Spectral Narrowing in All-Polymer Microcavities Doped with CdSe/CdS Dot-in-Rod Nanocrystals". In: *ACS Photonics* 4 (7 July 2017), pp. 1761–1769. ISSN: 23304022. DOI: 10.1021/acsphotonics.7b00330.

[47] Heba Megahd et al. "All-Polymer Microcavities for the Fluorescence Radiative Rate Modification of a Diketopyrrolopyrrole Derivative". In: *ACS Omega* 7 (18 May 2022), pp. 15499–15506. ISSN: 24701343. DOI: 10.1021/acsomega.2c00167.

[48] Boxuan Gao et al. "Design, fabrication and characterization of a distributed Bragg reflector for reducing the étendue of a wavelength converting system". In: *Optics Express* 28 (9 Apr. 2020), p. 12837. ISSN: 10944087. DOI: 10.1364/oe.391080.

[49] Sophocles J. Orfanidis. *Electromagnetic Waves and Antennas*. URL: http://eceweb1.rutgers.edu/~orfanidi/ewa/.

[50] Braxton Osting. "Bragg structure and the first spectral gap". In: *Applied Mathematics Letters* 25 (11 2012), pp. 1926–1930. ISSN: 08939659. DOI: 10.1016/j.aml.2012.03.002.

[51] Paola Lova, Giovanni Manfredi, and Davide Comoretto. *Advances in Functional Solution Processed Planar 1D Photonic Crystals*. Dec. 2018. DOI: 10.1002/adom.201800730.

[52] Konstantinos S. Daskalakis et al. "Converting an Organic Light-Emitting Diode from Blue to White with Bragg Modes". In: *ACS Photonics* 6 (11 Nov. 2019), pp. 2655–2662. ISSN: 23304022. DOI: 10.1021/acsphotonics.9b01206.

[53] Manpreet Singh et al. *Emerging cytokine biosensors with optical detection modalities and nanomaterial-enabled signal enhancement*. Feb. 2017. DOI: 10.3390/s17020428.

[54] Jiao Wang et al. *Optical microcavities with tubular geometry: Properties and applications*. 2014. DOI: 10.1002/lpor.201300040.

[55] *Strong light-matter coupling with 2D materials Starke Licht-Materie Kopplung mit 2D Materialien*.

[56] Cheng Zhang, Huijie Li, and Dong Liang. "Antireflective vertical-cavity surface-emitting laser for LiDAR". In: *Nature Communications* 15 (1 Dec. 2024). ISSN: 20411723. DOI: 10.1038/s41467-024-44754-w.

[57] Daniel Najer et al. "A gated quantum dot strongly coupled to an optical microcavity". In: *Nature* 575 (7784 Nov. 2019), pp. 622–627. ISSN: 14764687. DOI: 10.1038/s41586-019-1709-y.

[58] Xinyu Ma et al. "Integrated microcavity electric field sensors using Pound-Drever-Hall detection". In: *Nature Communications* 15 (1 Dec. 2024). ISSN: 20411723. DOI: 10.1038/s41467-024-45699-w.

[59] D S Jones et al. *ELECTRICAL AND MECHANICAL OSCILLATIONS An Introduction*. 1961.

[60] Manuel Hertzog et al. *Strong light-matter interactions: A new direction within chemistry*. Feb. 2019. DOI: 10.1039/c8cs00193f.

[61] LibreTexts. *The Quantum Harmonic Oscillator*. URL: https://phys.libretexts.org/Bookshelves/University_Physics/University_Physics_(OpenStax)/University_Physics_III_-_Optics_and_Modern_Physics_(OpenStax)/07%3A_Quantum_Mechanics/7.06%3A_The_Quantum_Harmonic_Oscillator.

[62] Colorado University. *The Hamiltonian operator*. URL: https://physicscourses.colorado.edu/phys5250/phys5250_fa19/lecture/lec07-hamiltonian/.

[63] Takahito Oyamada et al. "Optical properties of oligo(9,9-diarylfluorene) derivatives in thin films and their application for organic light-emitting field-effect transistors". In: *Journal of Physical Chemistry C* 111 (1 Jan. 2007), pp. 108–115. ISSN: 19327447. DOI: 10.1021/jp0654056.

[64] Manuela Russo et al. "One-pot synthesis of polymer/inorganic hybrids: Toward readily accessible, low-loss, and highly tunable refractive index materials and patterns". In: *Journal of Polymer Science, Part B: Polymer Physics* 50 (1 Jan. 2012), pp. 65–74. ISSN: 08876266. DOI: 10.1002/polb.22373.

[65] Stefan Bachevillier et al. "Fully Solution-Processed Photonic Structures from Inorganic/Organic Molecular Hybrid Materials and Commodity Polymers". In: *Advanced Functional Materials* 29 (21 May 2019). ISSN: 16163028. DOI: 10.1002/adfm.201808152.

[66] Ayse Turak. "On the Role of LiF in Organic Optoelectronics". In: *Electronic Materials* 2 (2 June 2021), pp. 198–221. ISSN: 26733978. DOI: 10.3390/electronicmat2020016.

[67] Felipe A. Angel, Jason U. Wallace, and Ching W. Tang. "Effect of lithium and silver diffusion in single-stack and tandem OLED devices". In: *Organic Electronics* 42 (Mar. 2017), pp. 102–106. ISSN: 15661199. DOI: 10.1016/j.orgel.2016.12.023.

[68] Kyul Han et al. "Dual enhancing properties of LiF with varying positions inside organic light-emitting devices". In: *Organic Electronics* 9 (1 2008), pp. 30–38. ISSN: 15661199. DOI: 10.1016/j.orgel.2007.07.005.

[69] Ossila. *Dip Coating: Practical Guide to Theory and Troubleshooting*. URL: https://www.ossila.com/pages/dip-coating.

[70] Zhao Zhang, Fei Peng, and Konstantin Kornev. "The Thickness and Structure of Dip-Coated Polymer Films in the Liquid and Solid States". In: *Micromachines* 13 (7 June 2022), p. 982. ISSN: 2072-666X. DOI: 10.3390/mi13070982.

[71] Michael A. Papachatzakis. *Code for the automation of the Dip-coater*. URL: https://github.com/Michael-a-pap/dip_coater_mod.

[72] J.A.Woollam. *The VASE ellipsometer*. URL: https://www.jawoollam.com/products/vase-ellipsometer.

[73] Stéphane Kéna-Cohen, Stefan A. Maier, and Donal D.C. Bradley. "Ultrastrongly coupled exciton-polaritons in metal-clad organic semiconductor microcavities". In: *Advanced Optical Materials* 1 (11 Nov. 2013), pp. 827–833. ISSN: 21951071. DOI: 10.1002/adom.201300256.

[74] LaurentNevou. *Light-wave Transmission*. URL: https://github.com/LaurentNevou/Light_WaveTransmission1D.

[75] Mikko Salomäki. *Ellipsometer from the department of Chemistry*. URL: https://www.jawoollam.com/products/vase-ellipsometer.

[76] Ossila. *Ossila Dip-coater Datasheet*. URL: https://downloads.ossila.com/manuals/dip-coater.pdf.

[77] Justin M. Conley et al. "Developmental toxicity of Nafion byproduct 2 (NBP2) in the Sprague-Dawley rat with comparisons to hexafluoropropylene oxide-dimer acid (HFPO-DA or GenX) and perfluorooctane sulfonate (PFOS)". In: *Environment International* 160 (Feb. 2022). ISSN: 18736750. DOI: 10.1016/j.envint.2021.107056.

[78] European Chemical Agency. *Per- and polyfluoroalkyl substances (PFAS)*. URL: https://echa.europa.eu/hot-topics/perfluoroalkyl-chemicals-pfas.